Progress In Electromagnetics Research C, Vol. 122, 121–139, 2022

Research on Characteristics of Planar Coil Based on Grounding Grid Breakpoint Magnetic Coupling Detection Method

Weihua Cheng[1], Zhiquan Ye[1, *], Shiwei Jin[2], Shuai Wang[1], and Haitao Hou[1]

Abstract—Magnetic coupling detection method, as one of the methods of solving grounding grid breakpoint location problem, has the problem that the size of the transmitting coil is too large to be easily applied to the actual environment detection. In order to reduce the size of the transmitting coil and ensure the effect of breakpoints detection, this paper studies the characteristics of the planar coil based on the method of grounding grid breakpoint magnetic coupling detection. Firstly, a mathematical model of the planar coil magnetically coupled detection grounding grid breakpoint system under high frequency is established. After analyzing the model, factors of affecting the breakpoint detection effect and the high frequency characteristics of the system are derived. Secondly, a simulation model of the magnetically coupled detection grounding grid is established by using HFSS software. The influence of the line width, side length, number of turns, and turn spacing of the transmitting coil on the detection effect is studied in detail. Besides, according to the law, the coil size optimization design is carried out. At last, the experimental platform is built to verify the reliability of the simulation and theory. The results show that the detection effect decreases as the line width and side length of the planar coil decrease, but the effect of line width change is small. Increasing the number of turns and turn spacing can improve the coupling coefficient to increase the detection effect, but when the distortion region is located after the parallel resonance point, the distributed capacitance will greatly inhibit the detection effect.

1. INTRODUCTION

Grounding grid is an important facility to ensure the safe operation of the power system. Being buried underground for years by various microorganisms, chemical substances corrosion, primary battery effect, etc. causes corrosion or even breakage, resulting in weakened grounding performance and endangering the safety of personnel and power systems. Therefore, it is crucial to evaluate the corrosion degree of the grounding grid or find the breakpoints of the grounding grid.

The methods to diagnose grounding grid fault are divided into four main categories: electrical network method [1], electromagnetic field method [2, 3], electrochemical method [4, 5], and electrical impedance tomography method [6, 7]. The electromagnetic method is one of the more important methods. However, the electromagnetic effect between the grounding grid and the detection device needs enhancement in order to conduct accurate detection because there is a long distance between them. Moreover, serious magnetic field interference in the substation will also have a certain impact on the accuracy of the method [8]. Therefore, the coupling of the detection device and grounding grid is an effective way to solve the non-contact detection of grounding grid faults and avoid the influence of external magnetic field interference on the detection system.

Received 11 April 2022, Accepted 28 July 2022, Scheduled 8 August 2022
* Corresponding author: Zhiquan Ye (1044438698@qq.com).
[1] Faculty of Electrical and Control Engineering, Liaoning Technical University, Huludao, Liaoning 125105, China. [2] State Grid Liaoning Maintenance Company, Shenyang, Liaoning 110003, China.

Magnetically coupled resonant technology is one of the wireless power transmission technologies, which has the characteristics of coupling, long-range electrical energy transmission, and selectivity for frequency. This technology can achieve over-coupling under certain conditions. Frequency bifurcation phenomenon will occur when the system reaches over-coupling [9]. In recent years, many scholars have studied this phenomenon in detail. Paper [10] used two coils with different radii to eliminate the frequency bifurcation phenomenon, and the results showed that increasing the transmitting coil size could eliminate the frequency bifurcation as well as improve the transmission distance. Paper [11] found that the frequency bifurcation phenomenon also existed in the single-emission and double-receiving system through theoretical analysis and gradually disappeared as the distance between the transmitter and the receiver increased. Paper [12] found that increasing the radius of the primary coil and lateral movement of coils could effectively eliminate the frequency bifurcation phenomenon by establishing the mutual inductance formula of the lateral moving coil. Most of these results have studied the effect of frequency bifurcation on energy transmission and conducted proper design to suppress frequency bifurcation.

As a common phenomenon in magnetically coupled resonance technology, the related report about applying frequency bifurcation phenomenon to detection is less [13]. Tao has applied the magnetic coupling resonance and frequency bifurcation phenomenon to loop open-closed detection of grounding grid breakpoints [13]. However, it is just the start of exploring and studying, and the side length of the transmitting coil is the same as the side length of the single mesh of the grounding grid, which is $5\,\text{m} \times 5\,\text{m}$ and not conducive to be applied to the actual environmental detection.

Therefore, in order to reduce the size of the transmitting coil and ensure the detection effect of the breakpoint, this paper investigates the characteristics of the planar coil for magnetic coupling detection of the grounding grid breakpoint, focusing on the influence law of the planar coil line width, side length, number of turns, and turn spacing on the detection effect and the high frequency characteristics of the system, and optimizes the design of the planar coil size according to the variation law. Finally, the simulation results are verified by building an experimental platform.

2. PRINCIPLE OF MAGNETIC COUPLING DETECTION GROUNDING GRID

The principle of magnetic coupling detection grounding grid is that the coupling occurs between the transmitting coil on the ground and the mesh of the grounding grid, and the state information of the grounding grid is obtained by obtaining the phase-frequency curve of the transmitting coil, as shown in Figure 1. Each mesh of the grounding grid can be regarded as an inductance coil, which is equivalent to an RL circuit when the grounding grid mesh is not broken. When the mesh is broken, the break is equivalent to the introduction of a capacitor, which is equivalent to the formation of an RLC circuit at this time [13]. Magnetic coupling detection is to determine the state of the mesh of the grounding grid by detecting the RL circuit and RLC circuit.

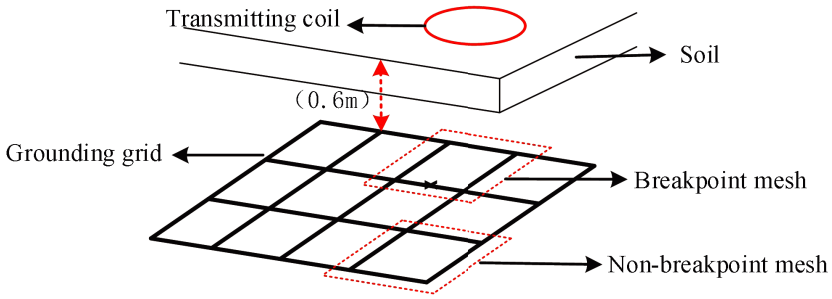

Figure 1. Schematic of magnetic coupling detection grounding grid.

2.1. Magnetic Coupling Detection Model at High Frequency

At present, the working frequency of magnetic coupling detection grounding grid system is high, usually above MHz [13]. In the case of high frequency, the performance of the inductor coil will change obviously,

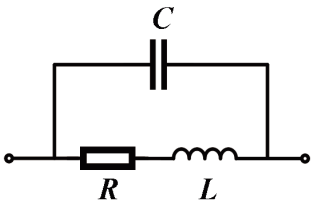

Figure 2. Equivalent model of transmitting coil at high frequency.

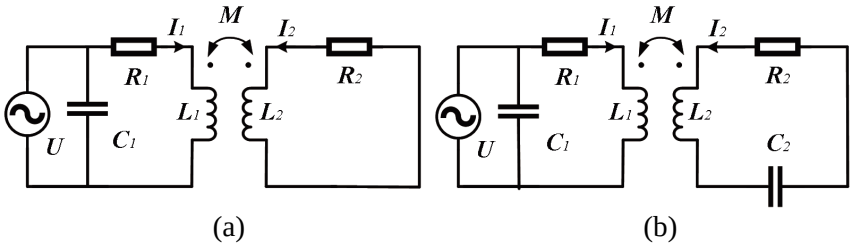

Figure 3. Equivalent circuit of detection system, (a) secondary coil RL circuit, (b) secondary coil RLC circuit.

and the distributed capacitance of the coil cannot be ignored. Its equivalent model is a parallel resonant circuit, as shown in Figure 2. R is the coil internal resistance, L the coil inductance, and C the distributed capacitance. The detected grounding grid mesh is equivalent to the secondary coil, and the two different states of the mesh with or without breakpoints correspond to different equivalent models of the circuit as shown in Figure 3. The secondary coil RL circuit in Figure 3(a) is the circuit model of the grounding grid without breakpoint, which is equivalent to an inductive wireless energy transfer circuit. The secondary coil RLC circuit in Figure 3(b) is the circuit model of the grounded grid with breakpoint, which is equivalent to the Magnetic Coupling Resonant Wireless Power Transfer (MCR-WPT) PS topology circuit.

In Figure 3, L_1 and L_2 are symbols of the inductance of the primary and secondary coils, respectively, and the internal resistances are R_1 and R_2; C_1 is the distributed capacitance of the primary coil; C_2 is the equivalent capacitance at the mesh break; M is the mutual inductance between the primary and secondary coils. It is pointed out in the literature [13] that when a break in the grounding grid occurs, the resonant frequency of the grounding grid is basically independent of the width and location of the break, that is, the equivalent capacitance of the break is basically constant.

When the distributed capacitance C_1 is not considered, the two circuits are obtained according to Kirchhoff's voltage law as:

$$\begin{cases} (R_1 + j\omega L_1)\,\dot{I}_1 + j\omega M\dot{I}_2 = \dot{U} \\ j\omega M\dot{I}_1 + (R_2 + j\omega L_2)\,\dot{I}_2 = 0 \end{cases} \tag{1}$$

$$\begin{cases} (R_1 + j\omega L_1)\,\dot{I}_1 + j\omega M\dot{I}_2 = \dot{U} \\ j\omega M\dot{I}_1 + \left(R_2 + j\omega L_2 + \dfrac{1}{j\omega C_2}\right)\dot{I}_2 = 0 \end{cases} \tag{2}$$

Formulas (1) and (2) are RL circuit and RLC circuit, respectively, and the impedance of the two systems without distributed capacitance is:

$$Z'_{rl} = R_1 + \frac{\omega^2 M^2 R_2}{R_2 + (\omega L_2)^2} + j\left(\omega L_1 - \frac{\omega^2 M^2 (\omega L_2)}{R_2 + (\omega L_2)^2}\right) \tag{3}$$

$$Z'_{rlc} = R_1 + \frac{\omega^2 M^2 R_2}{R_2^2 + \left(\omega L_2 - \dfrac{1}{\omega C_2}\right)^2} + j\left(\omega L_1 - \frac{\omega^2 M^2 \left(\omega L_2 - \dfrac{1}{\omega C_2}\right)}{R_2^2 + \left(\omega L_2 - \dfrac{1}{\omega C_2}\right)^2}\right) \tag{4}$$

Considering the distributed capacitance C_1, the total impedance of the two systems is:

$$Z_{rl} = \frac{1}{j\omega C_1 + \dfrac{1}{Z'_{rl}}} \tag{5}$$

$$Z_{rlc} = \frac{1}{j\omega C_1 + \dfrac{1}{Z'_{rlc}}} \tag{6}$$

From formulas (5), (6), the total impedances Z_{rl} and Z_{rlc} of the secondary coil RL circuit and RLC circuit will change with the change of the coil parameters. Moreover, the distributed capacitance C_1 will also have a great impact on the total system impedance.

2.2. Frequency Bifurcation Principle and Distortion Region Analysis

The frequency bifurcation phenomenon occurs in magnetically coupled resonant circuits. When resonance occurs, the imaginary part of the system input impedance is 0, and the magnetically coupled resonant systems is $\omega_0 = 1/\sqrt{L_1C_1} = 1/\sqrt{L_2C_2}$. When the PS topology system is in overcoupling, the three solutions generated by the frequency bifurcation can be derived from formula (6), that is, three resonant frequencies. The above cases are considered under the resonant frequency, that is, $\omega_0 = 1/\sqrt{L_1C_1} = 1/\sqrt{L_2C_2}$. However, most of the coupling between the transmitting coil and the grounding grid is not resonant but $1/\sqrt{L_1C_1} \neq 1/\sqrt{L_2C_2}$, which is a general coupling system at the time. According to the parameters of Table 1 and Table 2, the MATLAB calculation of formula (6) is carried out, the input impedance phase frequency curves at different C_2 in Figure 4 are obtained.

Table 1. Magnetic coupling system parameters.

Parameter	Value	Parameter	Value
R_1/Ω	1	M/μH	1
L_1/μH	10	R_2/Ω	1
C_1/pF	40	L_2/μH	10

Table 2. Resonant frequency of secondary coil at different C_2.

Parameter	Value			
C_2/pF	40	60	80	100
f_2/MHz	7.96	6.50	5.63	5.03

As seen in Figure 4, when the parameters are set and $\omega_0 = 1/\sqrt{L_1C_1} = 1/\sqrt{L_2C_2}$, frequency bifurcation occurs in the system. However, when $1/\sqrt{L_1C_1} \neq 1/\sqrt{L_2C_2}$, a distortion region similar to the frequency bifurcation also appears in the inputting impedance phase frequency characteristic curves, which is located near the resonance point of the secondary coil.

In the case of the same parameters, the input impedance phase frequency characteristic curves of the secondary coil RL circuit and the RLC circuit are compared as shown in Figure 5. From Figure 5, when the secondary coil is an RLC circuit, the phase frequency characteristic curve is distorted near the resonant frequency of the secondary coil. When the secondary coil is an RL circuit, the phase frequency characteristic curve has no obvious change. Therefore, we can judge whether the secondary coil is an RLC circuit or RL circuit through this distortion area, and then judge whether there is a break point in the grounding grid.

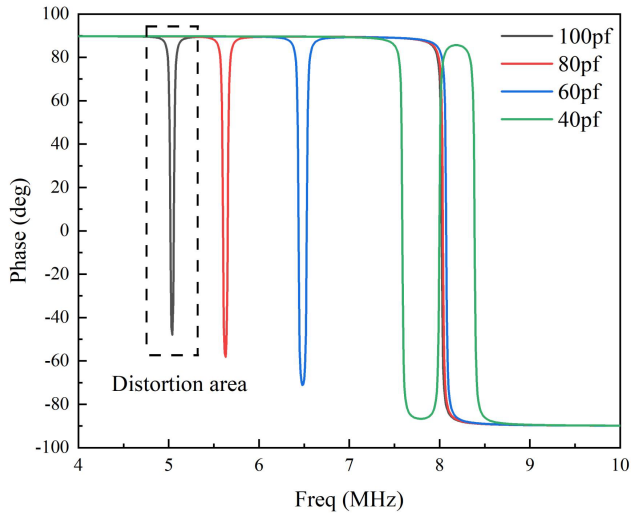

Figure 4. Input impedance phase frequency curve at different C_2.

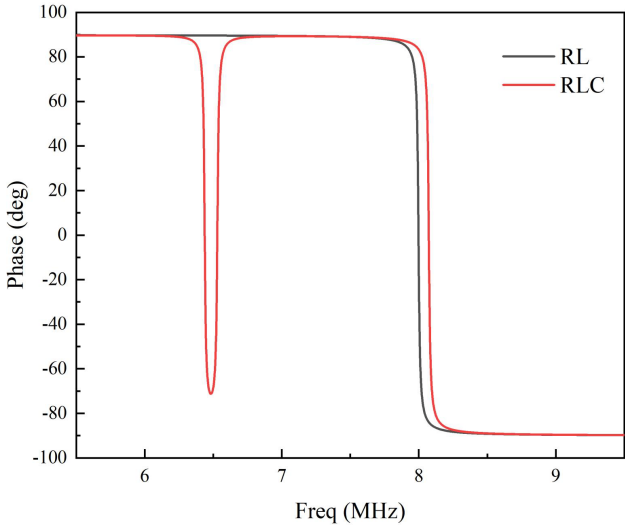

Figure 5. Input impedance phase frequency curve of secondary coil RL circuit and RLC circuit.

3. PLANAR COIL DETECTION GROUNDING GRID SYSTEM MODEL

It can be seen from formula (6) that when the parameters of the grounding grid are fixed, the detection effect of the magnetic coupling of the grounding grid is only related to the parameters such as self-inductance, mutual inductance, and distributed capacitance of the planar coil. Because the change of the geometric parameters of the planar coil will cause the change of these parameters at the same time, Formula (6) cannot directly reflect the detection characteristics of the planar coil to the breakpoint of the grounding grid in the magnetic coupling detection system. Therefore, this section establishes a mathematical model of the relationship between the geometric parameters of the planar coil and the magnetic coupling detection of the grounding grid, and analyzes the influence of line width and side length on the detection effect as well as the high-frequency characteristics of the system. In order to facilitate the calculation of the simulation software in the third section, the cross section of the transmitting coil is square, and the line width represents the side length of the section.

3.1. Coil Inductor

The calculation of the coil inductance consists of two parts: the self-inductance of each section of wire and the sum of the positive and negative mutual inductance between all sections of wire. The self-inductance of a planar spiral coil with a rectangular cross section can be expressed as [14]:

$$L_x = 2 \cdot l \cdot \left(\ln \frac{2 \cdot l}{w + t} + 0.50049 + \frac{w + t}{3 \cdot l} \right) \tag{7}$$

where L_x is the coil self-inductance in nH, l the coil wire length in cm, w the wire cross-section width in cm, and t the wire thickness in cm.

The mutual inductance in nH between the parallel lines of two adjacent segments of length l_i and l_j can be expressed as:

$$M_{i,j} = M\left(l_i + \delta\right) - M\left(\delta\right) \tag{8}$$

where:

$$\delta = \left| l_j - l_i \right| / 2 \tag{9}$$

$$M\left(l\right) = \frac{\mu_0}{2\pi} l \left\{ \ln \left[\frac{l}{d} + \sqrt{1 + \left(\frac{l}{d} \right)^2} \right] - \sqrt{1 + \left(\frac{d}{l} \right)^2} + \frac{d}{l} \right\} \tag{10}$$

d is the distance in cm between the centers of the two parallel lines.

The current direction decides the positive and negative mutual inductances between two parallel wires. The mutual inductance is positive for the same currents and negative for the opposite currents. Therefore, the positive and negative mutual inductances of the rectangular spiral coil are:

$$M_+ = \sum_{n=1}^{N} M_{y,y+4n} \tag{11}$$

$$M_- = \sum_{n=1}^{N} M_{y,y+4n-2} \tag{12}$$

y is the serial number of each line in Figure 6 (1, 2, 3, 4...), and N is the total number of lines. The final inductance of the whole rectangular spiral coil is:

$$L = L_x + M_+ - M_- \tag{13}$$

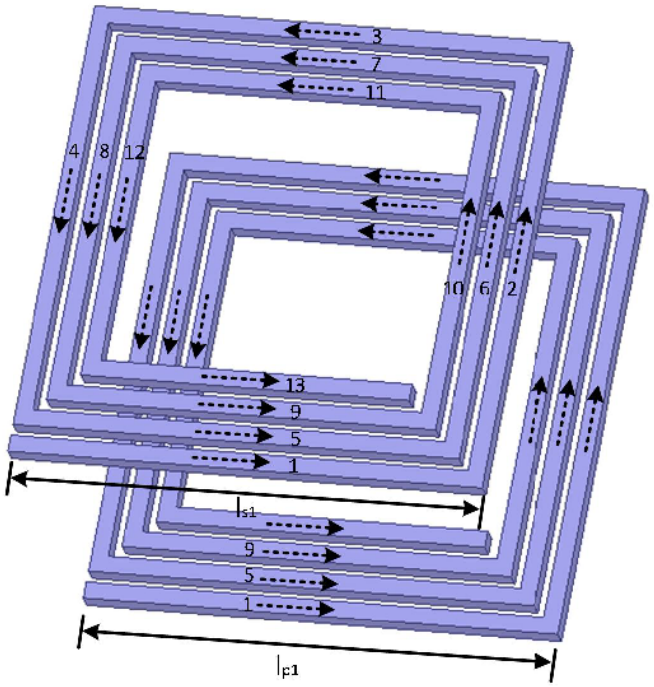

Figure 6. Mutual inductance between primary and secondary coils.

3.2. Coil Mutual Inductance

The total mutual inductance between the primary coil and the secondary coil can be considered as adding up the mutual inductance between segments. According to Figure 6, the lines with the same current direction are positive and with the opposite directions are negative. From Figure 6, the distance from each segment of the primary coil to the center of the rectangular coil can be calculated as:

$$d_1(i) = \frac{l_{p1} + l_{p2} + (-1)^i (l_{p1} - l_{p2})}{4} - \left\langle \frac{i-1}{4} \right\rangle (w_1 + s_1) \tag{14}$$

The distance of the secondary coils is:

$$d_2(i) = \frac{l_{s1} + l_{s2} + (-1)^i (l_{s1} - l_{s2})}{4} - \left\langle \frac{i-1}{4} \right\rangle (w_2 + s_2) \tag{15}$$

the subscripts 1 or p and 2 or s represent the relevant parameters for the primary and secondary coils, respectively. The total positive inductance can be written as:

$$M_+ = \sum_{i=1}^{n1}\sum_{j=1}^{n2}\sum_{k=1}^{4} M_{4(i-1)+k,4(j-1)-k} \tag{16}$$

The research in this paper only considers the case that the two coils are completely symmetrical along the center. The central distance between the primary coil and secondary coil can be written as:

$$d_+ = \sqrt{\{d_1[4(i-1)+k] - d_2[4(j-1)+k]^2 + D^2\}} \tag{17}$$

D represents the distance between the two coils along the central axis. The negative mutual inductance can be written as:

$$M_- = \sum_{i=1}^{n1}\sum_{j=1}^{n2}\sum_{k=1}^{4} M_{4(i-1)+k,4(j-1)-k+(-1)^k+5} \tag{18}$$

The distance between them can be written as:

$$d_- = \sqrt{\{d_1[4(i-1)+k] - d_2[4(j-1)-k+(-1)^k+5]\}^2 + D^2} \tag{19}$$

The total mutual inductance between the two coils is the difference value between the positive and negative mutual inductances as:

$$M = M_+ - M_- \tag{20}$$

3.3. Coil Resistance and Distributed Capacitance

At high frequency, the skin effect will make the AC resistance of the transmitting coil and the flat steel of the grounding grid increase. Since the grounding grid mesh resistance variation has a large impact on the detection effect, it should be considered. The AC resistance R_s can be written as:

$$R_s = R_{dc} \cdot \frac{t}{\delta \cdot \left(1 - e^{-t/\delta}\right)} \tag{21}$$

where:

$$\delta = \sqrt{\frac{2}{\omega\mu\gamma}} \tag{22}$$

δ represents the penetration depth (in m), ω the angular frequency $\omega = 2\pi f$, μ the magnetic permeability (in H/m), and γ the electrical conductivity (in S/m). At high frequency, the distributed capacitance of the coil cannot be ignored. The distributed capacitance will be generated between turns and turns, coil and ground. Because the distributed capacitance of the magnetic coupling detection system is more complex, this model does not calculate the distributed capacitance quantitatively. It is pointed out in [15] that the distributed capacitance increases with the decrease of turn spacing and the increase of gap length between parallel lines.

3.4. Plane Coil Detection Grounding Grid System Characteristics Analysis

The grounding grid is studied according to the square single mesh with buried depth of 0.6 m, size of 3 m × 3 m, and cross-sectional area of 60 mm × 5 mm. Because the actual parameters of the grounding grid are not easy to obtain by calculation, and this paper focuses on the characteristics of the coil, the parameters of the grounding grid are calculated as shown in Table 3, and the resonance point of the grounding grid can be obtained as 7.96 MHz from the parameters in Table 3. The MATLAB calculation is carried out according to formulas (6), (13), (20), and the step size of frequency scanning is 0.01 MHz. The influence of the change of coil geometric parameters on the phase frequency curve is obtained when the grounding grid is broken.

The effect of the distributed capacitance is not considered. Figure 7 represents the effect of changing the geometric parameters of the transmitting coil on the phase frequency curve. Figure 7(a) shows the effect of changing the line width on the phase frequency curve when the side length of the single-turn

Table 3. Parameters of grounding grid.

Parameter	R_2 (Ω)	L_2 (μH)	C_2 (pF)
Value	1	10	40

transmitter coil is constant at 1.5 m. Figure 7(b) shows the effect of changing the side length on the phase frequency curve when the line width of the single-turn transmitter coil remains constant at 6 mm. In the picture, different colors represent different phase angles. And the wider the distortion region is, the smaller the lowest phase angle is, and the better the detection effect is.

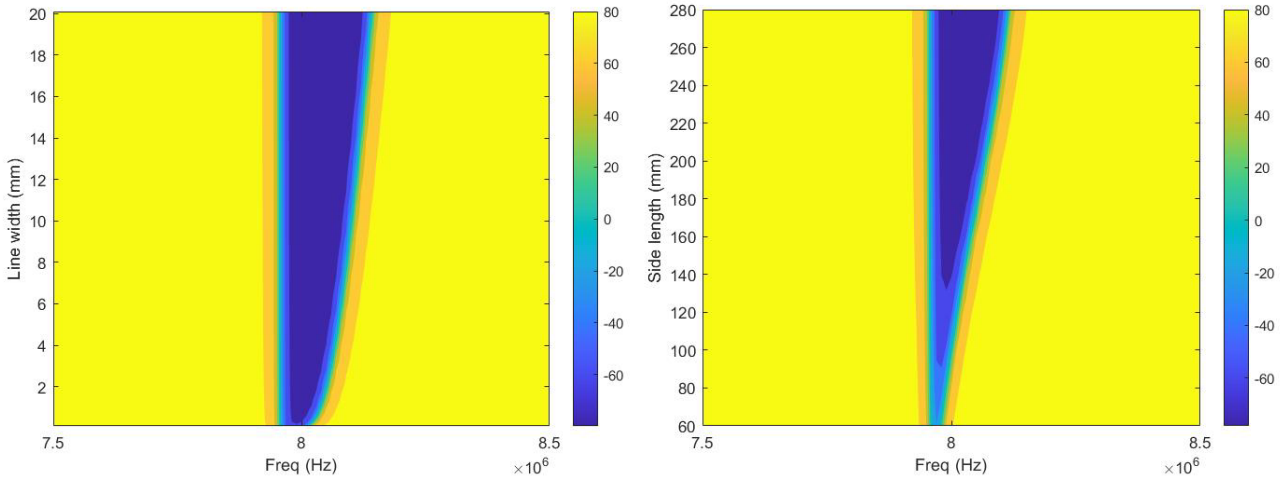

Figure 7. Effect of variation of transmitting coil geometric parameters on the phase frequency curve. (a) The effect of line width change on phase frequency curve. (b) The effect of side length change on phase frequency curve.

From Figure 7(a), the distortion region appears near 8 MHz (the resonance point of the secondary coil). When the side length is certain, as the line width decreases, the width of the distortion region decreases; the phase angle nadir increases; and the detection effect is weakened, but the degree of weakening is smaller. From Figure 7(b), when the line width is certain, without exceeding the size of the grounding grid mesh, as the side length decreases, the width of the distortion region decreases; the phase angle nadir increases, and the detection effect is weakened; and the weakening effect is more obvious.

Consider the high frequency characteristics of the system, that is, the effect of distributed capacitance on the detection effect. Figure 8 shows the effect of changing the distributed capacitance on the phase frequency curve when the geometric parameters of the transmitting coil are unchanged, with a single-turn side length of 3 m and a line width of 6 mm.

As can be seen in Figure 8, when the other parameters of the transmitting coil remain unchanged, the parallel resonance point moves forward with the increase of the distributed capacitance, so that the distortion region is located behind the parallel resonance point. The larger the distributed capacitance is, the less obvious the distortion area is, and the worse the detection effect is. The reason is that when the parallel resonance point is located behind the distortion region, it can be seen from the Equation (6) that the effect of distributed capacitance is greatly enhanced, which will restrain the appearance of the distortion region.

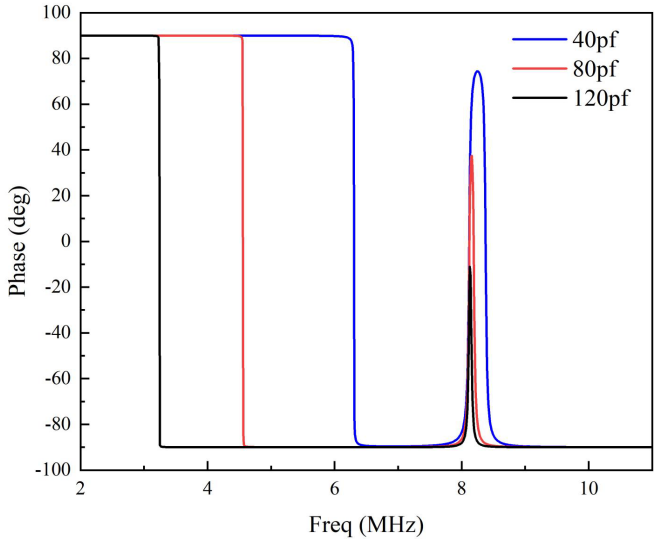

Figure 8. Effect of distributed capacitance on phase frequency curve.

4. SIMULATION MODEL

In order to verify the accuracy of the above mathematical model and research in more detail the effect of the variation of each geometric parameter of the transmitting coil on the detection effect, HFSS and ANSYS Maxwell simulation software were used for modeling and analysis. A simulation model of planar coil detecting the breakpoint of grounding grid was established as shown in Figure 9. The upper part is the square grounding grid mesh, and the lower part is the square transmitting coil. The height difference between the two is 0.6 m, simulating the detection of breakpoints of grounding grid with a burial depth of 0.6 m.

The grounding grid single mesh is used as the receiving coil, and its basic parameters are as follows: the material is galvanized flat steel; the side length is 3 m × 3 m; the thickness is 6 mm; the width is 50 mm; the fixed break width is 10 mm. The break location is shown in Figure 9, and the material parameters of galvanized flat steel in the simulation software are shown in Table 4. The sweep range

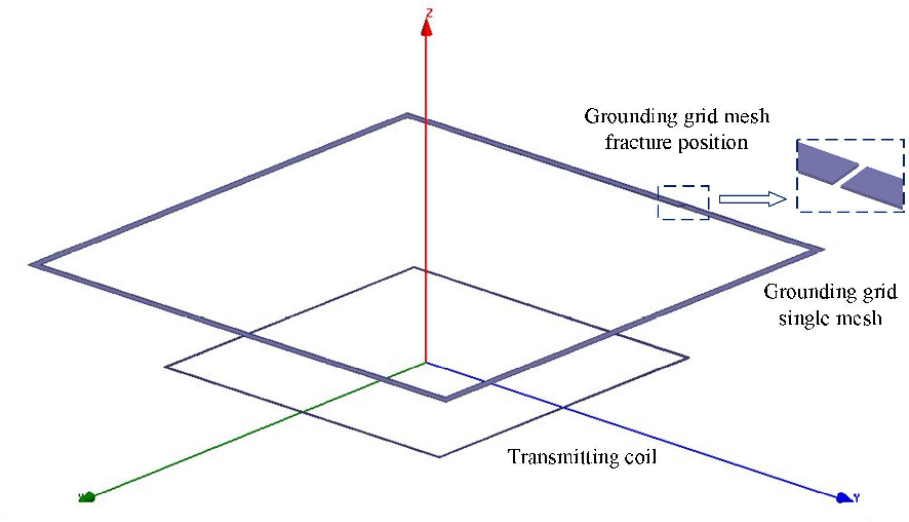

Figure 9. Simulation model of breakpoint of grounding grid with magnetic coupling detection.

Table 4. Parameters of galvanized flat steel [6, 16].

Parameter	Relative Permittivity	Relative Permeability	Bulk Conductivity	Dielectric Loss Tangent	Magnetic Loss Tangent
Value	1	636	6000000 siemens/m	0	0

in HFSS is 6–15 MHz, and the step size is 0.01 MHz. In order to facilitate the simulation calculation, the cross section of the transmitting coil is square, and the line width represents the side length of the section.

4.1. Influence of the Change of Coil Geometry Parameters on the Detection Effect of the System

The transmitting coil adopts a single turn. The side length is 1.4 m, and the line width ranges from 2 mm to 20 mm in steps of 2 mm to simulate. The influence of the change of the line width of the transmitting coil on the detection effect is studied. The parameters of the model are simulated and analyzed by ANSYS Maxwell.

From Figure 10, with the continuous increase of line width, the self-inductance of the transmitting coil gradually decreases; the mutual inductance remains basically unchanged; the coupling coefficient increases; and the overall enhancement of detection is enhanced, but the enhancement effect is small. The line width is from 2 mm to 20 mm, and the lowest point of the distortion region is only from 80° down to 72°. With the increase of the line width, the weight of the transmitting coil will increase in a square multiple. Therefore, if we want to improve the detection effect by increasing the line width, we need to consider the increase of the weight of the transmitting coil after increasing the line width.

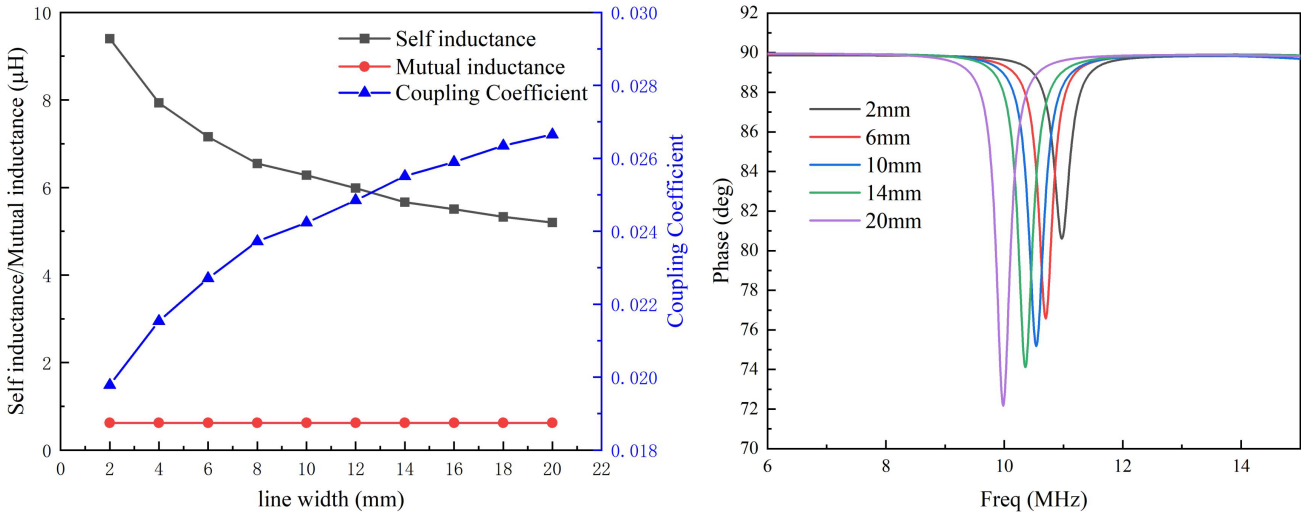

Figure 10. Parameter variation curve and phase frequency curve under different line width.

The transmitting coil is a single turn. The line width is 6 mm, and the side length is from 0.8 m to 4 m. The influence of the change of the side length of the transmitting coil on the detection effect is studied.

As can be seen from Figures 11(a) and (b), when the side length of the transmitting coil is between 0.8 m and 3 m, the self-inductance and mutual inductance increase as the side length increases, and the coupling coefficient also increases. The parallel resonance point of the transmitting coil decreases continuously. With the increase of coupling coefficient, the detection effect is enhanced.

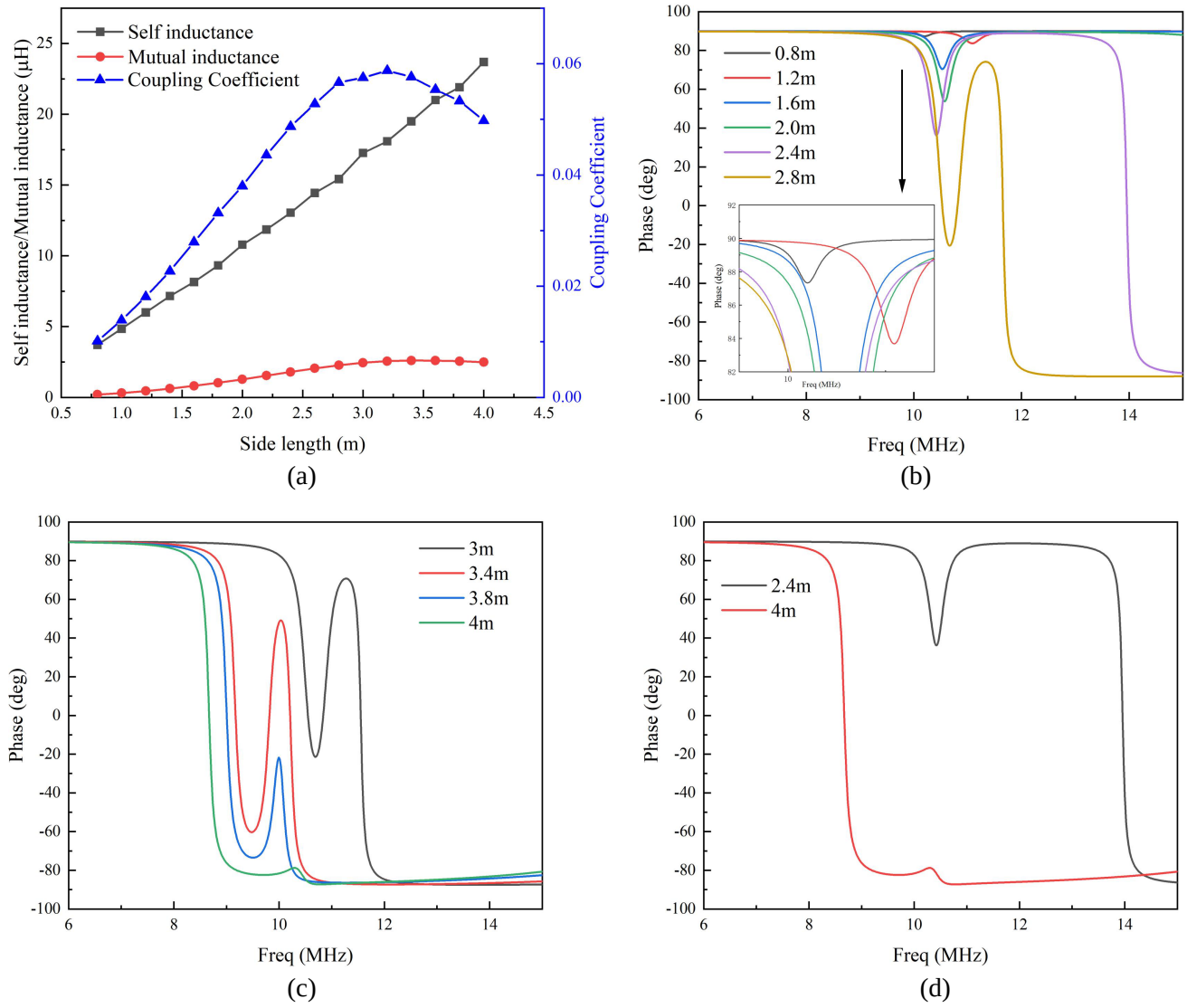

Figure 11. Parameter variation curves and phase frequency curves at different edge lengths. (a) The values of each parameter at different side lengths. (b) Phase frequency curve of side length 0.8 m–3 m. (c) The phase frequency curve of side length 3 m–4 m. (d) Phase frequency curves for side lengths of 2.4 m and 4 m.

As can be seen from Figure 11(c), after the side length exceeds 3 m, the self-inductance increases, and the parallel resonance point decreases as the side length increases, making the distortion region located after the parallel resonance point of the transmitting coil. The detection effect can be seen to be weakened. As seen in Figures 11(a) and (d), when the side lengths of the transmitting coil are 2.4 m and 4 m, the coupling coefficients are 0.049 and 0.058, respectively, and the latter is slightly higher than the former. But the lowest points of distortion region are 54° and 11°, respectively, and there is a great difference between them. The reason for the appeal phenomenon is that the coupling coefficient of the whole system keeps decreasing after the side length exceeds 3 m, which causes the weakening of the detection effect. Another reason is that the distributed capacitance of the coil will affect the detection effect at higher frequencies. As the coil side length increases, the self-inductance increases, and the parallel resonance point decreases, making the distortion region located after the parallel resonance point of the transmitting coil, and the distributed capacitance has an increasing effect on the detection, which suppresses the appearance of the distortion region. The above phenomenon verifies the reasonableness

of the mathematical model at higher frequencies in the second chapter.

The width of the transmitting coil is 6 mm; the side length is 1.4 m; the turn spacing is 10 mm; and the number of turns from 1 to 4 turns is simulated to study the effect of the change in the number of turns of the transmitting coil on the detection effect.

As can be seen from Table 5, with the increase of the number of turns, the self-inductance and mutual inductance continue to increase, and the coupling coefficient of the system also increases. With the increase of the number of turns, the distributed capacitance is also increased, so that the parallel resonance point is greatly reduced, and the inhibitory effect of the distributed capacitance is greatly enhanced. As a result, the distortion region of the 1-turn coil with small coupling coefficient in Figure 12 is larger than that of the 2-turn coil, and there is no obvious distortion region after more than 2 turns.

The transmitting coil line width is 6 mm; the side length is 1.2 m; the number of turns is 2 turns; and the turn spacing is simulated from 8 to 40 mm in steps of 8 mm to study the effect of the change of the turn spacing of the transmitting coil on the detection effect.

From Table 6, it can be seen that with the increase of turn spacing, the self-inductance is increased,

Table 5. Parameters after the change of number of turns.

Number of turns	Self-inductance (μH)	Mutual inductance (μH)	Coupling Coefficient
1	6.78137	0.59718	0.02239
2	20.54255	1.16645	0.02518
3	40.24007	1.70827	0.02640
4	64.85403	2.22343	0.02708

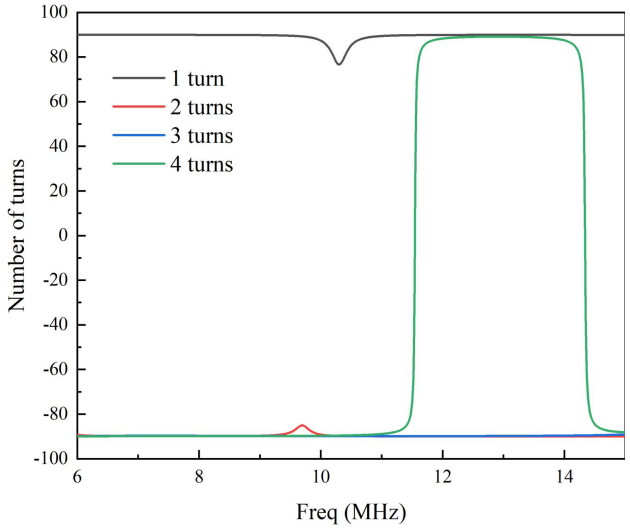

Figure 12. Phase frequency curve after the number of turns change.

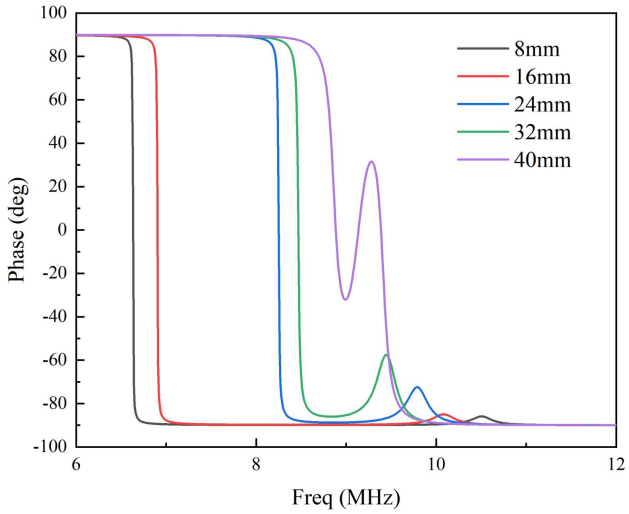

Figure 13. Phase frequency curve after the change of turn spacing.

Table 6. Parameters after the change of turn spacing.

Turn spacing (mm)	Self-inductance (μH)	Mutual inductance (μH)	Coupling Coefficient
8	17.70151	0.88807	0.02064
16	16.80869	0.87607	0.02089
24	16.16157	0.86432	0.02103
32	15.69515	0.85271	0.02107

and the coupling coefficient is also increased. It can be seen from Figure 13 that the distributed capacitance is decreased with the increase of turn spacing, so that the parallel resonance point becomes larger; the inhibitory effect of distributed capacitance becomes smaller and smaller; and the detection effect is getting better and better.

4.2. Coil Optimization and Design

Based on the above study of the influence of the geometric parameters of the planar coil on the magnetic coupling detection system, in order to reduce the size of the transmitting coil and ensure the detection effect of the breakpoint, it is necessary to optimize and design the parameters of the coil. The coupling coefficient between the optimized coil and the grounding grid should be higher in order to improve the detection effect, and the parallel resonance point should not be too small to prevent the suppression of the distortion area by the distributed capacitance. For this reason, the optimal design flow of planar coil is proposed, as shown in Figure 14. Because the line width change has little effect on the detection effect, the optimization process does not change the line width. In the figure, r represents the side length, N the number of turns, and a the turn spacing (maximum 100 mm). If there is no coil that can meet the requirements of the effect in the change of turn spacing from 10 mm to 100 mm after increasing the number of turns, the optimization process ends. According to the actual grounding grid size, the minimum size planar coil can be designed according to the coil optimization design process.

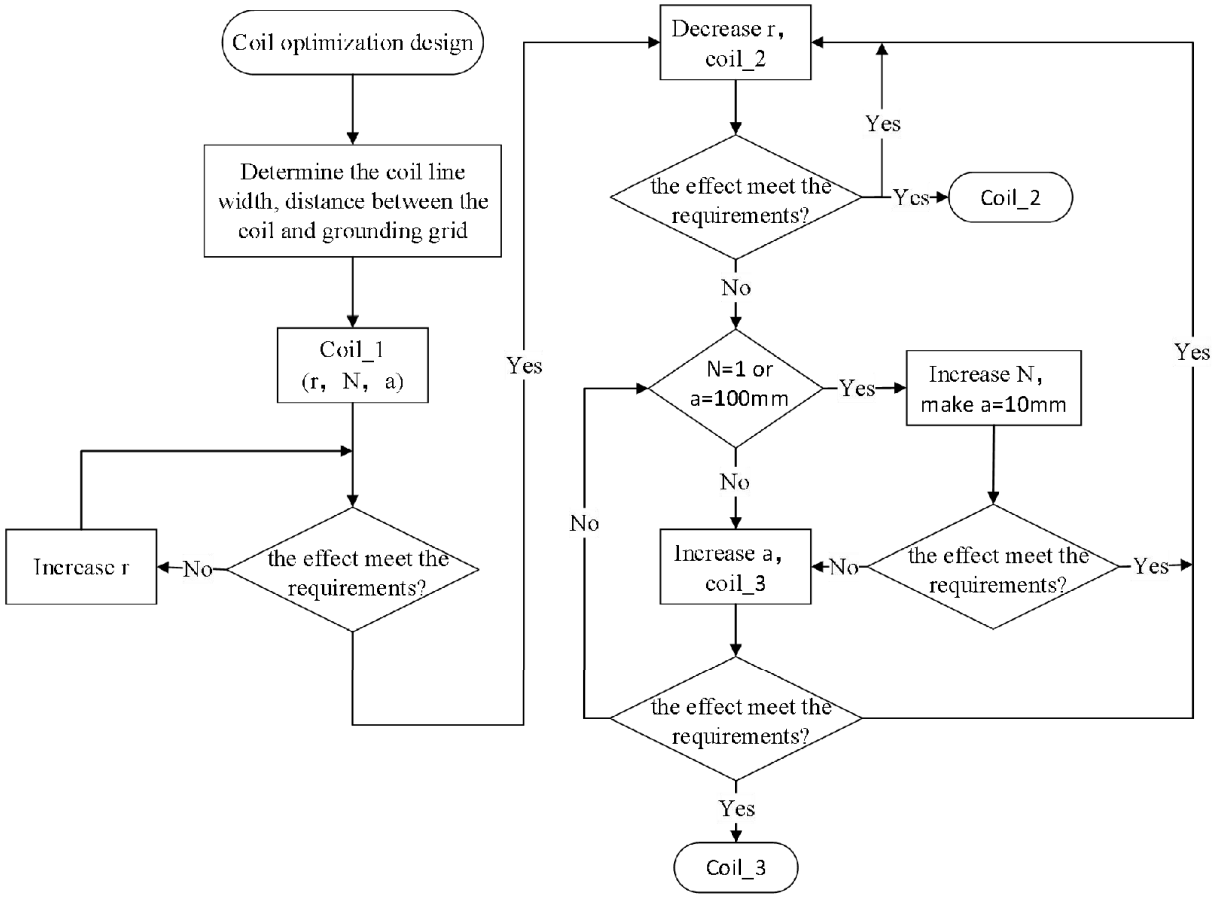

Figure 14. Design flow chart of the minimum coil that meets the testing requirements.

The specific coil optimization design process is shown as follows: Firstly, assure the coil line width and the distance between the coil and the grounding grid, then determine the initial coil side length, number of turns and turn spacing. The number of turns and turn spacing are initially 1 turn and

10 mm. When the initial coil meets the effect requirements, the operation of reducing the coil side length is performed until the effect cannot meet the requirements. When the requirement is not met, and the number of turns is 1 turn, or the turn spacing is 100 mm, the operation of increasing the number of turns with the initial turn spacing 10 mm is performed. If the effect meets the requirement, repeat the operation of reducing the side length. If the effect still meets the requirement after reducing the side length, continue to reduce the side length, and update the parameters of coil_2 to the latest coil parameters. If the effect does not meet the requirement after increasing the number of turns, then increase the turn spacing until the turn spacing increases to 100 mm, and then increase the number of turns. Finally, the coil with the smallest size is selected by comparing coil_2 and coil_3.

In this section, the optimized design of the transmitting coil is carried out for 2×2 grounding grid with specific parameters according to the single mesh parameters of the grounding grid. The simulation study is carried out in HFSS simulation software, and the simulation model is shown in Figure 15. The detection effect requires that the absolute value of the difference between the lowest point or the highest point of the distortion region and the non-distortion area (90° or −90°) is more than 5°. The line width here is set to 6 mm; the initial side length r is 1700 mm; the number of turns is 1 turn; and the turn spacing is 10 mm. According to the optimized design flow in Figure 15, the difference values shown in Table 7 are obtained after simulation. As can be seen from Table 7, when the coil has 1 turn, with

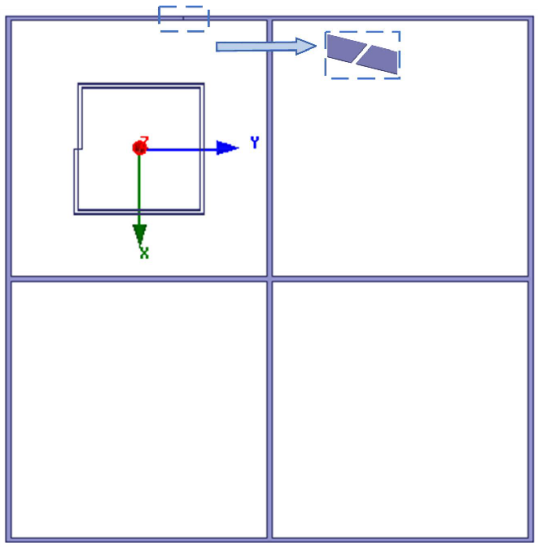

Figure 15. 2×2 grounding grid simulation model.

Table 7. Difference between distortion region and non-distortion region.

Side length (mm)	Number of turns and turn spacing							
	1 turn	2 turns						3 turns
		$a = 10$ mm	$a = 15$ mm	$a = 20$ mm	$a = 25$ mm	$a = 30$ mm	$a = 35$–100 mm	$a = 10$–100 mm
1700	9.1							
1600	6.4							
1500	5.7							
1400	5.6							
1300	3.7	3.5	8.3					
1250			0	5.9				
1200				0	0	21.0		
1150						0	0	0

the side length decreases, the difference becomes smaller and smaller, that is, the detection effect gets weaker and weaker. When the number of turns is 2, the distortion region is located behind the parallel resonance point. It can be seen from the table that the detection effect is getting better and better with the increase of turn spacing. After optimization, the planar coil parameters of minimum size are: side length 1200 mm, number of turns 2, and turn spacing 30 mm. The side length is reduced to 0.4 times that of the single mesh of the grounding grid.

5. EXPERIMENT

In order to verify the law of the influence of planar coil parameters on the detection effect, an experimental platform as shown in Figure 16 was established according to the simulation model diagram in Figure 9. The whole detection system includes KEYSIGHT 33500B signal generator, Aigtek ATA-1220D broadband amplifier, KEYSIGHT DSOX1204A oscilloscope, and resonance compensation circuit. The receiving coil used Φ2 mm varnished wire with a square coil of size 20 cm $\times$ 20 cm to simulate a single mesh of grounding grid. The transmitting and receiving coils are 40 mm apart. In the experiment, the waveforms of the voltage and current of the transmitting coil are measured directly by an oscilloscope. The frequency of the signal generator is adjusted to the working frequency of the system; the voltage is adjusted to 2.5 Vpp; the sine wave is output; and the gain of the broadband amplifier is adjusted to 20 dB. By adjusting the frequency of the signal generator several times (in steps of 0.1 MHz), the phase difference between voltage and current at different frequencies was recorded to obtain the phase difference graph of the transmitting coil. Because the size of the transmitting and receiving coils is small, the parallel resonance point and distortion region are after 100 MHz, which is not convenient for experiment. In this experiment, the parallel capacitor of the transmitting coil and the series capacitor of the receiving coil are used to reduce the frequency of the parallel resonance point and distortion region.

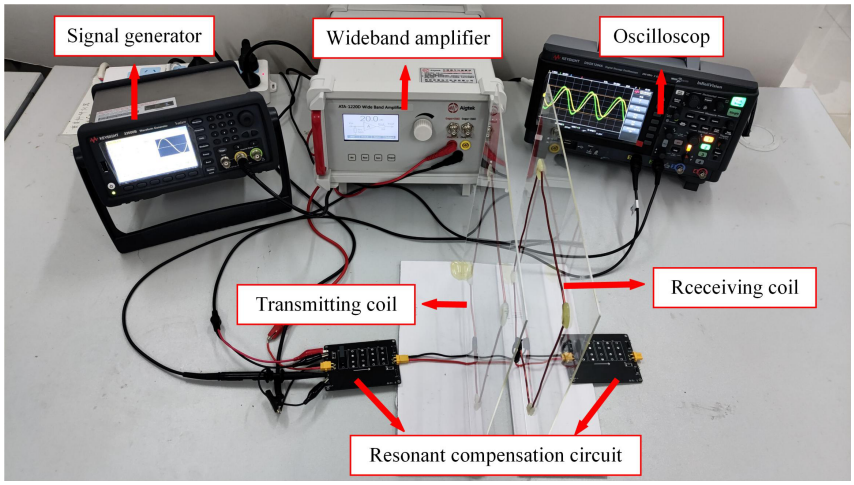

Figure 16. Experimental platform.

Without considering the effect of distributed capacitance, that is, no parallel capacitance, the inductance of the receiver coil is 769 nH; the series capacitance is 1.5 nf; and the resonance point is 4.7 MHz by calculation. The transmitting coil is a square coil with the size of 20 cm $\times$ 20 cm and the line widths of 0.5 mm, 1 mm, 2 mm, and 4 mm, respectively. The relevant coil parameters are shown in Table 8.

As can be seen in Figure 17, with the increase of line width, the general trend of the lowest point of distortion region gets lower and lower, and the detection effect gets better and better. The difference between the lowest point of distortion region of line width 0.5 mm and line width 4 mm is 13°.

The influence of the change of the side length of the transmitting coil on the detection effect is

Table 8. Parameters for different line widths.

	Size	Number of turns	Line width (mm)	Self-inductance (nH)
Receiving Coil	20 cm × 20 cm	1	2	769
Transmitting coil	20 cm × 20 cm	1	0.5	1084
	20 cm × 20 cm	1	1	915
	20 cm × 20 cm	1	2	773
	20 cm × 20 cm	1	4	655

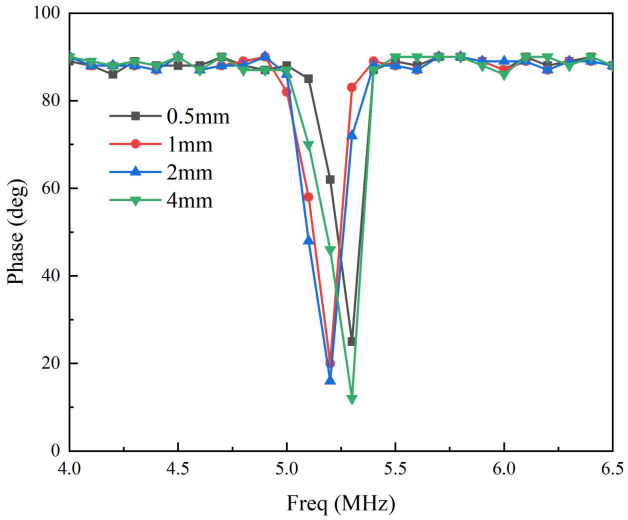

Figure 17. Phase frequency curve after line width change.

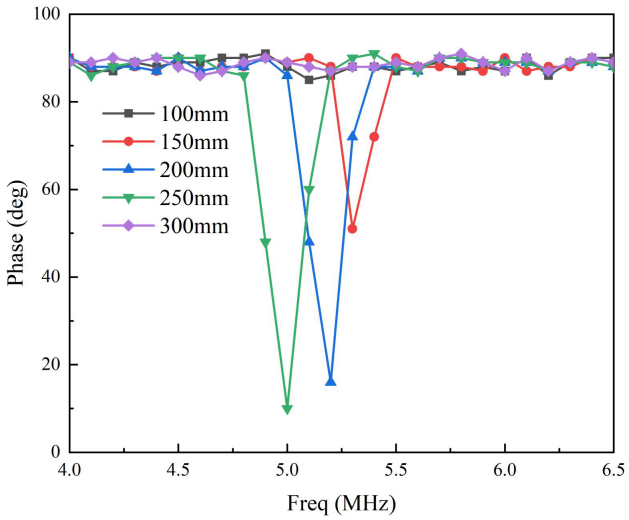

Figure 18. Phase frequency curve after side length change.

studied. The transmitting coil is a square coil with the line width of 2 mm and the side lengths of 10 cm, 15 cm, 20 cm, 25 cm, and 30 cm, respectively. The relevant coil parameters are shown in Table 9.

Figure 18 shows that when the side length of the transmitting coil is smaller than the grounding grid mesh, the lowest point of the distortion region becomes lower and lower with the increase of the side length of the transmitting coil, and the detection effect becomes better and better. No distortion region appears for the transmitting coil with side length of 100 mm. When the edge length increases from 150 mm to 200 mm, the lowest point of the distortion area decreases from 51° to 16°. When the side length of the transmitting coil exceeds the grounding mesh, the coupling coefficient decreases, and the detection effect is weakened. As in Figure 18, no distortion area appears when the side length is 300 mm. The detection effect is better for the 250 mm coil than the 200 mm coil in Figure 18, which

Table 9. Parameters for different side lengths.

	Size	Number of turns	Line width (mm)	Self-inductance (nH)
Receiving coil	20 cm × 20 cm	1	2	769
Transmitting coil	10 cm × 10 cm	1	2	330
	15 cm × 15 cm	1	2	530
	20 cm × 20 cm	1	2	773
	25 cm × 25 cm	1	2	1015
	30 cm × 30 cm	1	2	1268

may be due to the manual winding error of the coil, or the scanning step 0.1 MHz cannot find the lowest point of the actual distortion area.

In order to verify the inhibitory effect of distributed capacitance on the detection effect in the high frequency case, this place uses the transmitting coil parallel capacitor to reduce the parallel resonance point and facilitate the experiment, which is convenient for the experiment. Both the grounding grid mesh and the transmitting coil are made of 20 cm × 20 cm varnished wire with a line width of 2 mm. The parallel capacitances of the transmitting coil are 1.5 nf, 2 nf, 2.5 nf, 3 nf, and 4 nf, respectively.

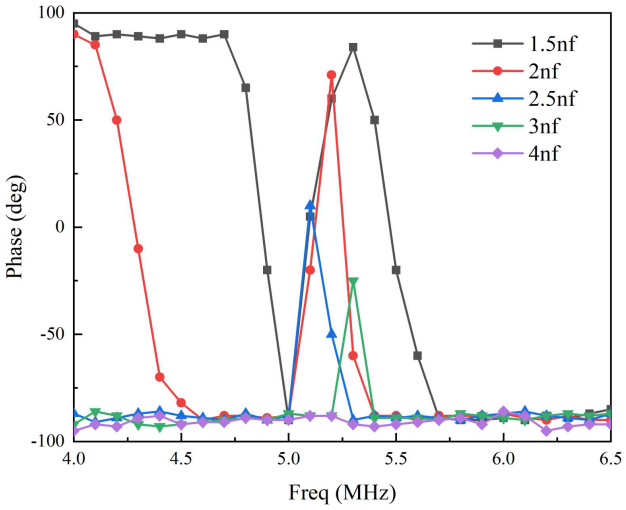

Figure 19. Phase frequency curve after the change of distributed capacitance.

As can be seen from Figure 19, when the value of the parallel capacitance increases, which is equivalent to the increase of the distributed capacitance, the parallel resonance point moves forward; the highest point of the distortion region gradually decreases; and the detection effect becomes worse and worse. When the distributed capacitance increases from 1.5 nf to 3 nf, the highest point of the distortion region decreases from 84° to −25°, and the distortion region can no longer be detected when the distributed capacitance is 4 nf. The experiment shows that when the distributed capacitance increases, and the distortion region is after the parallel resonance point, the distributed capacitance will greatly suppress the distortion region, causing the detection effect to be greatly weakened. The correctness of the mathematical model of magnetic coupling detection grounding grid at high frequency in the paper is verified.

6. CONCLUSION

In order to reduce the size of the transmitting coil while ensuring the detection effect, the characteristics of the planar coil based on the magnetic coupling detection grounding grid breakpoint system are studied in this paper. The mathematical model of magnetic coupling detection in high frequency case is analyzed, and the law of the influence of the change of line width, side length, number of turns, and turn spacing of the planar coil on the magnetic coupling detection system is studied in detail by HFSS and Maxwell simulation software. The coil is reasonably optimized and designed according to the law. Finally, the reliability of the simulation and theory is verified by building an experimental platform. The main work and conclusions of this paper are as follows:

(1) The mathematical model of the grounding grid with magnetic coupling detection under high frequency is established, and the impedance expressions of the grounding grid with and without breakpoints in two cases are derived; the principle of the grounding network with magnetic coupling detection breakpoints and the distortion region are analyzed, and the condition for judging whether there is a breakpoint or not is found.

(2) By establishing a mathematical model of the relationship between the geometric parameters of the planar coil and the magnetic coupling detection of the grounding grid, the influence law of the change of line width and side length on the detection effect is quantitatively analyzed, and the high-frequency characteristics of the system are studied. The results show that the distributed capacitance of the coil in the high-frequency case is not negligible and will have a suppressive effect on the distortion region. When the distributed capacitance increases from 40 pf to 120 pf, the difference between the distortion region and the normal region decreases from 164° to 79°.

(3) The magnetic coupling detection grounding grid model was established by HFSS and Maxwell simulation software, and the law of the influence of the change of the geometric parameters of the planar coil on the magnetic coupling detection system is studied in detail. As the line width and side length of the transmitting coil increase, the coupling coefficient increases, and the detection effect becomes better and better; however, when the side length exceeds the size of the grounding grid, the larger the side length is, the smaller the coupling coefficient is, and the worse the detection effect is. When the distortion region is located after the parallel resonance point, the distributed capacitance will have a suppression effect on the distortion region, and the farther the distance is, the greater the suppression effect is. Finally, the coil is optimized and designed for 2×2 grounding grid, and the side length of the optimized coil was reduced to 2/5 of the side length of the single mesh of the grounding grid.

(4) An experimental platform for the magnetically coupled detection grounding grid system was built to verify the reliability of the simulation and theory.

ACKNOWLEDGMENT

This research was supported by the Natural Science Foundation of Liaoning Province (No. 2021MS338).

REFERENCES

1. Wang, S., J. Liu, S. Wang, and Z. Li, "Grounding grid corrosion diagnosis and uncertainly analysis of branches," *Journal of Computers*, Vol. 5, No. 8, 1289–1295, 2010.
2. Yu, S., G. Dong, N. Liu, X. Liu, Y. Ji, and H. Luan, "Diagnosis for conductor breaks of grounding grids based on the wire loop method of the transient electromagnetic method," *Mathematical Problems in Engineering*, Vol. 2019, 1–11, 2019.
3. Yu, C., Z. Fu, G. Wu, L. Zhou, and X. Zhu, "Configuration detection of substation grounding grid using transient electromagnetic method," *IEEE Transactions on Industrial Electronics*, Vol. 64, No. 8, 6475–6483, 2017.
4. Li, J., H. Su, F. Chai, D. M. Xue, L. Li, X. Y. Li, and H. M. Meng, "Corrosion behavior of low-carbon Cr micro-alloyed steel for grounding grids in simulated acidic soil," *Journal of Iron and Steel Research International*, Vol. 25, No. 7, 755–766, 2018.
5. Shao, Y., M. Mu, and Z. Bing, "Corrosion behavior of copper-clad steel bars with unclad two-end faces for grounding grids in the red clay soil," *Journal of Materials Engineering & Performance*, Vol. 26, No. 4, 1–7, 2017.
6. Yan, X., Q. Lyu, X. Lin, and W. Chen, "Research on grounding grid electrical impedance tomography algorithm based on Tikhonov and TV hybrid regularization," *Chinese Journal of Scientific Instrument*, Vol. 42, No. 11, 160–171, 2021.
7. Yan, X., X. Lin, Q. Lyu, and W. Chen, "Grounding grid electrical impedance tomography based on Homotopy-Tikhonov algorithm," *Transactions of China Electrotechnical Society*, 1–13, 2021.
8. Fu, Z., X. Wang, Q. Wang, X. Xu, N. Fu, and S. Qin, "Advances and challenges of corrosion and topology detection of grounding grid," *Applied Sciences*, Vol. 9, No. 11, 2290, 2019.
9. Niu, W. Q., J. X. Chu, W. Gu, and A. D. Shen, "Exact analysis of frequency splitting phenomena of contactless power transfer systems," *IEEE Transactions on Circuits and Systems I: Regular Papers*, Vol. 60, No. 6, 1670–1677, 2012.
10. Lyu, Y. L., F. Y. Meng, G. H. Yang, B. J. Che, Q. Wu, D. Erni, and L. W. Li, "A method of using nonidentical resonant coils for frequency splitting elimination in wireless power transfer," *IEEE Transactions on Power Electronics*, Vol. 30, No. 11, 6097–6107, 2015.

11. Li, W., H. Zhang, C. Li, and L. Ding, "Analysis of transmission characteristics of single-emission and double-receiving system based on magnetic resonant coupling," *Transactions of China Electrotechnical Society*, Vol. 29, No. 2, 191–196, 2014.
12. Han, R., T. Wang, and Z. Zhao, "Study of wireless power transfer system frequency bifurcation phenomenon and elimination method," *Electric Machines and Control*, Vol. 24, No. 5, 116–123, 2020.
13. Tao, Y., "Analysis of loop on-off detection based on magnetic resonance frequency splitting," MA thesis, Chongqing University, 2018.
14. Greenhouse, H. M., "Design of planar rectangular microelectronic inductors," *IEEE Transactions on Parts Hybrids & Packaging*, Vol. 10, No. 2, 101–109, 1974.
15. Jow, U. M. and M. Ghovanloo, "Design and optimization of printed spiral coils for efficient transcutaneous inductive power transmission," *IEEE Transactions on Biomedical Circuits and Systems*, Vol. 1, No. 3, 193–202, 2007.
16. Yu, Y., Z. Zhu, Z. Zhang, S. Huang, J. Xia, and C. Gao, "Research on material selection of transmission tower grounding body," *Materials Science & Technology*, Vol. 24, No. 5, 25–31, 2017.